Untethered Near-Field Drone Based Antenna Measurement System for Microwave Frequencies using Multiple Reference Antennas for Phase and Drone Location Recovery

Clive G. Parini, Stuart F. Gregson and Anthony K. Brown

Abstract: **The simulation of a novel drone-based NF/FF antenna measurement system enabling the reconstruction of AUT phase and the true location of the untethered drone using multiple land-based reference antennas is described. The mathematical approach follows the principle used within GPS position and time recovery. Conceptually the satellites are replaced by ground based reference antennas of known location, the user location is now the drone location and the user clock offset is replaced by the unknown AUT phase radiated at the angle subtended between the AUT and drone location. This addresses the need for drone based NF/FF antenna measurement of large in-situ VHF/UHF antenna arrays plus the need to measure the installed performance of microwave antennas on structures such as buildings, aircraft and ships. To assess the viability a computer simulation of the measurement system is constructed and its performance analysed in terms of the accuracy of reconstruction of the AUT phase and true drone location, as well as the NF/FF radiation pattern accuracy in terms of Equivalent Multipath Level (EMPL). An example measurement 'range', comprising AUT location and six fixed REF antennas demonstrates wide AUT operating bandwidth of (0.5 to 2) GHz, with EMPL < -50dB over the forward hemisphere.**

I. INTRODUCTION

As is widely recognised, the exponential growth in use of the wireless spectrum is giving major concern over system characterisation in a real-world deployed environment. This is equally true in communications, radar and IOT applications. What is required is an accurate determination of radiating performance in "real world" conditions. This need results from the proliferation of competing and coexisting antenna technologies placed on a given outdoor platform. These devices may either be physically large themselves such as VHF arrays used in radio astronomy or become large and/or are immovable when placed in situ along with their accompanying supporting structures including objects as varied and complex in form as buildings, towers, trains, ships, aircraft, etc. Measuring the FF radiation pattern and gain of large antennas using 'airborne' sources is not new, for example [24] reports the measurement of the gain of large (30m) earth station antennas using celestial radio sources to accuracies of ±0.45dB. For these types of antenna with very low-noise receivers, radiation patterns can be measured with a sensitivity of about 15 to 20dB below beam-axis response, adequate for beamwidth measurement but unable to resolve important sidelobe detail [32]. The sun can also be used but has complex emission characteristics and like all celestial sources is a wideband source requiring very narrow band receivers. Use of single drones (UAV) for antenna measurements (either as source or receiver) has been growing in recent years [1] and typically occur over broad frequency bands but more commonly at lower frequencies (below 1GHz) [2]. Example measurements include the characterisation of fixed, phased array antennas at a few MHz to several hundred MHz which cannot be readily characterised within an anechoic chamber due to their size and frequency range. The use of drone-based measurements for such structures has gained increasing interest due in part to the agility, convenience, and cost effectiveness of drone-based technology. Measurements currently reported are most commonly made directly in the far-field, although development of measurement strategies in the near-field is progressing [3]. This early work has led to a growth in understanding of the use of drones in these types of measurement applications, most recently including polarisation characterisation. The work of [4] offers a highly comprehensive study of the errors and uncertainty sources of far-field (FF) drone based measurements, in this case undertaken at 14.5GHz with an offset reflector AUT with gain of order 30 dBi. Outdoor slant range antenna pattern measurements taken at both 35° and 45° AUT elevation angles with drone transmitting ranges of 350m and 700m are reported and compared with reference patterns obtained from spherical near-field measurements made at the ESA-ESTEC test facility. Both co-polar and x-polar antenna pattern measurements were performed and levels of Equivalent Error Signal (difference between drone measured amplitude pattern and reference pattern) of -56dB (co-polar azimuth) and -48dB (x-polar azimuth) were achieved.

There are clear limitations to the current drone measurement technologies however. For electrically large objects or antennas operating at VHF, the height limitations of typical drones (120m in the UK) are such they will normally be in the near-field of these antennas. Also, in the case of large antenna farms it is often not possible to tilt an antennas elevation down sufficiently low for unobstructed slant range FF drone based measurements. Near-field (NF) drone measurements are thus needed, but have been limited to date by the need to measure both amplitude *and* phase. As is known [5] the ultimate limit to the accuracy in a NF measurement system is dominated by both the positional and phase accuracy. Currently used NF techniques include flying an optical fibre cable tether to provide the phase reference [6,7,8], as well as using phase retrieval techniques with multiple amplitude scans at different NF distances [9,27],

which have both measurement time and accuracy penalties for physically large structures. Tethered systems offer good performance and [29] describes a 2.45GHz measurement of an 8dB gain horn AUT using a laser tracker to determine the drone-based probe location and a tethered optical fibre for phase reference. NF phase accuracy was better than 9° and the transformed FF pattern exhibited pattern errors of <-30dB. However, the tether is a severe limitation to the inherent flexibility offered by free flying drones.

Phase retrieval techniques measure the antenna near-field amplitude on two concentric surfaces and are post-processed by means of iterative techniques to recover phase information. If only a radiation pattern cut is required then [26] describes a ground-based amplitude only phase retrieval system where just two concentric NF rings are measured, the complex far-field for the corresponding ring plane being retrieved. This avoids the full two-dimensional scanning of traditional near-field measurements if only a radiation pattern cut is required. In this case the phase retrieval algorithm benefits from the reduced dimensionality of the problem as the number of unknowns have been reduced to a single ring, improving the performance compared to standard full spherical phase retrieval approaches. In [26] experimental results with a 35dB gain reflector antenna indicated -44dB Equivalent Multipath Level (EMPL) [5] for this approach compared to -37dB EMPL for a full spherical phase retrieval measurement. In our experience the limitation of this approach is that the AUT radiation pattern should not vary much with distance in the orthogonal axis for successful results. In addition, [26] shows that for these phase retrieval approaches to be this effective the first measurement ring needs to be at 15-30% of the AUT FF distance and the second ring radius needs a separation of at least another 25%. For many applications these are unacceptably large distances for drones in terms of both flight altitude and flight time limitations and negate the compact measurement space that true NF offers. In [27] a method to make both the amplitude only plane measurements simultaneously with a single drone flight by mounting two receive antenna at the front and rear of the drone separated by 0.8m (12.4λ) and so performing a two-plane measurement at a distance of 70λ and 82.4λ. With the AUT FF distance being 124λ this means the two planes were at 56% and 66% of the FF distance, outside the optimal locations suggested by [26]. Measured results presented for this drone-based system were compared with those made in an anechoic chamber using both a single complex surface and two amplitude only surfaces. Both phase retrieval derived FF patterns were clearly inferior to the single NF complex surface results, with considerable main beam radiation pattern distortion at levels as high as -16dB from boresight, indicating high EMPL levels.

In [28] the authors state that "Most methods tackling the phase retrieval problem of magnitude-only antenna measurements suffer from unrealistic sampling requirements, from unfeasible computational complexities, and, most severely, from the lacking reliability of nonlinear and nonconvex formulations". In terms of reliability [28] suggests that applying conventional NF phase retrieval characterization to two similar unknown AUTs the procedure may arbitrarily fail for one set of data while it may provide accurate results for the other AUT. Mathematical evaluation of the conventional phase retrieval process in [28] leads its authors to conclude that it remains a highly nonlinear task with inherent lack of reliability. They also conclude that phase retrieval measurements "need to be carried out with higher precision, e.g., larger SNR and lower positioning uncertainty, than their coherent counterparts in order to obtain results of similar accuracy". For the above reasons we believe that surface-to-surface phase retrieval techniques are not suitable for drone based measurements with EMPL levels below circa -30dB. As an alternative, [28] proposes a partially coherent multiprobe measurement technique where a small array of drone mounted receive antennas with receivers that measure the NF amplitude and measure the NF phase relative to one of the array elements. The phase retrieval process success is then considerably improved by adding this localized phase information in form of phase differences among neighbouring measurement samples. For our requirements, that need to go down to 50MHz, this novel approach is impractical in terms of drone deployment of the array.

For low frequency AUTs [30] describes a 175MHz measurement system where the phase of the transmitting drone is determined through the use of a single fixed ground-based reference receiving antenna. Unlike in conventional ground-based FF measurement system where the reference antenna is fixed and located close to the AUT positioner, here the distance (and hence phase) between drone probe and the reference antenna changes with each NF measurement point. To recover the transmitted phase the use of Differential GPS (DGPS) is used to first fix the location of the reference antenna and then the location of the drone probe. From this geometry the probe reference antenna path length can be determined, and along with compensation for the radiated phase patterns of probe and reference antennas, the transmitted probe phase is determined. Measured results showed that the average NF phase error was <14°. This error is largely due to the *frequency independent* error associated with DGPS location accuracy (2 x 2 x 5) cm in (x, y, z) [4] which at 175MHz would be as much as 12°. Whilst this is a useful approach for this low frequency application, moving to say 1.75GHz would mean the DGPS error alone would increase to as much as 120°, which corresponds to l/3 of a wavelength which is about seven times larger than the typically accepted minimum accuracy of 1/20 of a wavelength.

Another class of NF/FF drone-based measurements being considered for array antennas [11] uses a simulation-based model of the current distribution on an a priori known antenna array which is then modified to match the measured data. In principle, this can help to reduce the number of required samples and the measurement time, or to improve the resilience of the reconstructed pattern to probe positioning errors. However, to date, significant errors are introduced related to reliability of the simulations due in part to uncertainty on the precise antenna geometry of actual manufactured arrays.

As mentioned above, another limitation to employing NF/FF methods is the positional accuracy to which the drones are known (including the polarisation alignment), which limits their use at higher microwave frequencies. The development of irregular sampled antenna NF/FF transformation algorithms, see for example chapter 10 of [5], has been key to enabling NF drone measurements where the key drone performance parameter is the accurate determination of its position in 3D space. Techniques for this include differential GPS [4], laser tracker [7,13], Real-Time Kinematic (RTK) positioning [14]. Drone location accuracies of order several centimetres have been practically achieved with laser trackers offering potentially (0.1 to 0.5) mm accuracy but as yet unproven in this class of application especially in uncontrolled outdoor settings. Issues include being able to track flying drone dynamics [7,19], in terms of the drone mounted laser targets field of view, useable range (40m) and the targets weight (1Kg) when an auto tracking target is deployed. In addition, the need for line-of-sight between the laser tracker on ground and the laser target installed on the drone during a complete NF acquisition (and the need to avoid the laser tracker looking directly into the sun) would limit the ability to scan the AUT in its installed environment.

In this paper we report a novel alternative NF/FF approach to measure the phase of the AUT and the true location of the drone through the use of multiple land-based reference antennas. The approach is based around the principle of GPS in that the known location of four or more satellites transmitting time-stamped signals to a user enables the four unknowns of the user (x, y, z) location plus the users clock offset from the satellites synchronised GPS time to be determined. In this approach the satellites are replaced by ground based reference antennas of known location, the user location is now the drone and the user clock offset is replaced by the unknown AUT radiated phase pattern received at the drone location, *i.e.* the NF phase at the sample point. This work is motivated by the need to develop a drone based highly flexible NF/FF antenna measurement system capable of measuring VHF/UHF antenna array elements and RF combined sub-arrays for radio-astronomy applications as well as the installed performance as part of the commissioning process of microwave antennas on structures such as buildings, aircraft and ships at frequencies of up to tens of GHz.

In section 2 of the paper we describe the theory behind the measurement process and in section 3 we build a simulation of the proposed NF/FF drone measurement system and evaluate its performance both in terms of the accuracy of the recovered NF phase plus reconstructed drone location as well as the quality of the transformed FF radiation pattern in terms of the EMPL. The paper is completed in section 4 where we draw some conclusions and present our suggestions for the planned further work.

II. AUT PHASE AND DRONE POSITION RECONSTRUCTION FROM FOUR OR MORE REFERENCE ANTENNA PHASE MEASUREMENTS

As described in the introduction, the proposed measurement system is based around the principals of GPS. Here the VNA measured phase difference between one of four (or more) reference antennas and the AUT when the system is illuminated by the transmitting drone provide four (or more) equations in the four unknowns of the AUT phase and the unknown coordinates of the drone, enabling these unknowns to be solved. Such VNAs are commercial off the shelf products (COTS) and are available from a number of suppliers operating, for example, to 40 GHz with up to 24 channels and are relatively inexpensive and portable [16,17]. A diagram showing the proposed measurement system is shown in Fig. 1.

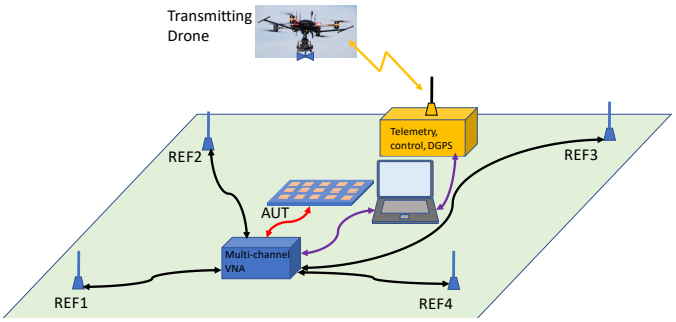

Fig. 1. Drone measurement concept showing the minimal four REF antennas and equipment setup along with an array antenna as AUT.

Here, the multichannel VNA enables the phase difference between the signal received from the drone by the AUT and the signal received from the drone by each REF antenna to be measured simultaneously with a trigger from the control system. The true location of the drone is P at coordinates (t_x, t_y, t_z) and this we aim to determine along with the unknown AUT phase, ϕ_{AUT}. The system also records the differential GPS (DGPS) location of the drone, termed P' at coordinates (d_x, d_y, d_z).

Consider the general NF/FF process in terms of a transmitting probe and receiving AUT with the AUT being an aperture antenna (e.g. reflector or array antenna). The transmitting probe located say at a point near the edge of the AUT aperture excites just a small portion of the AUT aperture and the amplitude and phase received at the AUT output port is the antennas response to that partial aperture excitation. Once all such samples are obtained the NF/FF process then formulates a suitable mode spectrum, which in the case of planar NF is the plane-wave spectrum, formulated about an AUT cartesian coordinate frame whose origin is usually (but not necessarily) some physical point on the AUT structure. It is to this origin point that the transformed FF pattern (as well as the back-projected AUT aperture illumination) is computed [33]. In the context of this work this AUT origin point is the location of the AUT and the phase response of the AUT at a given probe location is the unknown phase that this technique aims to retrieve. As in any NF/FF system the probe must be outside the reactive NF of the AUT for the process to be valid. The probe to AUT aperture distance may be in the probe NF or FF and this fact is taken account of by the probe compensation part of the NF/FF process [33].

Fig. 2 shows a possible test set up, with the drone at its true location, P. Then, the pathlength difference expressed as a phase difference, ϕ'_{Rn}, between the signal from the drone at P to the AUT at coordinates (a_x, a_y, a_z), and the drone to the n^{th} REF antenna, R_n, at coordinates (r^n_x, r^n_y, r^n_z), is given by:

$$\phi'_{Rn} = k\,R_n - (k\,D - \phi_{AUT}) \quad (1)$$

where:

$$\boldsymbol{R_n} = \sqrt{(\boldsymbol{t_x} - \boldsymbol{r_x^n})^2 + \left(\boldsymbol{t_y} - \boldsymbol{r_y^n}\right)^2 + (\boldsymbol{t_z} - \boldsymbol{r_z^n})^2}$$

and:

$$\boldsymbol{D} = \sqrt{(\boldsymbol{t_x} - \boldsymbol{a_x})^2 + \left(\boldsymbol{t_y} - \boldsymbol{a_y}\right)^2 + (\boldsymbol{t_z} - \boldsymbol{a_z})^2}$$

with k the free-space wavenumber and using a positive ($+j\omega t$) time-convention.

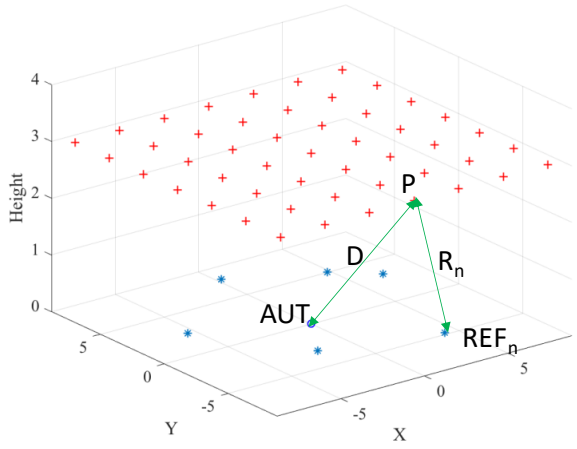

Fig. 2. Drone measurement set-up: AUT (blue circle) surrounded by 6 REF antennas (blue stars), and 49 NF drone measurement points (red crosses); Example of path lengths D and R1 are also shown. All dimensions in meters.

The path difference expressed as a phase, ϕ'_{Rn}, consists of the measured phase, ϕ_{Rn}, and an unknown number of full wavelengths N_n, thus,

$$\phi'_{Rn} = \phi_{Rn} + 2\pi N_n \quad (2)$$

However, we have a strong estimation of N_n from knowledge of the DGPS location of the drone $P'(d_x, d_y, d_z)$, giving:

$$\boldsymbol{N_n} = \mathbf{int}\left[\boldsymbol{k(R'_n - D')}/\boldsymbol{2\pi}\right] \quad (3)$$

with 'int' representing the integer function and where:

$$\boldsymbol{R'_n} = \sqrt{(\boldsymbol{d_x} - \boldsymbol{r_x^n})^2 + \left(\boldsymbol{d_y} - \boldsymbol{r_y^n}\right)^2 + (\boldsymbol{d_z} - \boldsymbol{r_z^n})^2}$$

and:

$$\boldsymbol{D'} = \sqrt{(\boldsymbol{d_x} - \boldsymbol{a_x})^2 + \left(\boldsymbol{d_y} - \boldsymbol{a_y}\right)^2 + (\boldsymbol{d_z} - \boldsymbol{a_z})^2}$$

If we choose a measurement frequency such that the DGPS error is less than or equal to the wavelength, then the true value of N_n will be known to within ±1. Thus, for the case of four REF antennas, equation (1) forms a set of four simultaneous equations in the four unknowns of the true location of the drone $P(t_x, t_y, t_z)$ and the AUT phase, ϕ_{AUT}. These equations can be solved using the Newton-Raphson method [18,15]. Since N_n is only known to within ± 1 of its true value we need to attempt trial solutions with all possible combinations from N_1-1, N_2-1, N_3-1, N_4-1 through N_1, N_2, N_3, N_4 to N_1+1, N_2+1, N_3+1, N_4+1, which in this case is 81 possible combinations. We can judge the quality of the resulting solution by looking at the residuals from the Newton-Raphson/method, and seeking the lowest values. As in the analogous case of GPS, we can use more than the minimal four REF antennas to improve the robustness of the solution and in this case we can apply the method of Least Squares to solve for the four unknowns [18], again judging the quality of the solution by seeking the lowest set of residues. For the case of five REF antennas the number of combinations of (N_n - 1) to (N_n +1) we need to test for a solution increases to 243, and for six REF antennas this increases to 729.

The above formulation assumes that:

i) We can accurately determine the physical locations of the phase centres of the REF antennas relative to a reference point, (a_x, a_y, a_z,) on the AUT aperture. In practice, the REF antenna will have a physical reference point marked on it and the phase centre is *a priori* known to that point. The Cartesian coordinates of the REF antennas relative to (a_x, a_y, a_z) can then be measured using, for example, a Total Station Theodolite (TST). A typical TST can measure distances up to 1,500 metres with an accuracy of about 1.5 mm ± 2 parts per million [19]. This is accomplished by the TST using a modulated infrared carrier signal, the distance being determined by emitting and receiving multiple frequencies, and measuring the integer number of wavelengths to the target for each frequency, *cf.* ranging in Doppler radars. Alternatively, the use of a laser tracker potentially offers submillimetre accuracy [31].

ii) The differential GPS (DGPS) location of the drone $P'(d_x, d_y, d_z)$ is determined relative to the phase centre of the drone transmitting antenna. In practice the DGPS location will be made relative to a datum on GPS module attached to the drone, and so a translation to the drone antenna phase centre needs to be made. The reconstructed true drone location $P(t_x, t_y, t_z)$ is thus made relative to the drone transmit antenna phase centre.

iii) The drone transmit antenna is a dual polarised probe antenna which always points towards the AUT. This is achieved by mounting both transmit antenna and camera on a gimbal platform and employing object recognition software via onboard single board computer (Adreno type) to enable the camera (and hence antenna) to track the AUT, Fig. 1. This avoids the need for any probe compensation due to the drone transmit antenna radiation pattern [5]. However, we assume that the drone transmit antenna pattern would have a low gain omni-directional radiation pattern in the forward hemisphere to keep physical size and weight small, and to ensure a sufficiently strong signal illuminates all the REF antennas at every location of the drone as it transverses the synthesised NF measurement surface. Ideally NF/FF transformation requires both hands of polarisation to be measured at the SAME point and the use of a dual polarised probe with fast signal switching between polarisations ensures that the NF data can be collected in a single pass.

iv) The REF antenna should ideally exhibit a flat phase function of the type typically used as GPS antennas. However, correction for the REF antenna polarisation and its phase pattern as a function of radiation angle is possible within the formulation.

III. A MATLAB SIMULATION OF THE DRONE MEASUREMENT SYSTEM

In order to evaluate the viability of the proposed drone measurement system described in Section 2 a simulation of the measurement process was constructed in MATLAB. The basic experimental system is depicted in Fig. 2, which shows the case where the AUT is surrounded by six reference antennas (blue stars). The drone transmits the microwave test signal at each of the 49 designated NF measurement points (red crosses), of which one, at point P, is shown in the figure. From point P the transmitted signal is received by the AUT and all the REF antennas, and the multiport Vector Network Analyser (Fig.1) simultaneously measures the phase difference between the AUT (connected to the VNA reference port) and each of the REF antennas, hence measuring the path difference $D - R_n$ (for the nth REF antenna) as a phase, ϕ_{Rn}. Multiport VNAs are standard instruments these days and as an example we site the Rohde & Schwarz ZNBT [16], which offers from 8 to 24 ports. The accuracy to which this phase, ϕ_{rn}, can be measured will be a factor in the system performance and as a baseline we have taken this accuracy to be 2° RMS (the effect of this parameter is studied later in the paper). To produce the errored phase we use a uniformly distributed random number generator which yields a peak-to-peak variation in phase of ±3.5° for the 2° RMS setting. The accuracy to which we can place the drone at a desired measurement point is dependent on the accuracy of the DGPS employed on the drone and the ground segment equipment. In [4] it is suggested that the accuracy to which a drone using DGPS can be placed is 2cm in x and y and 5cm in z (zenith). In the simulation we thus place the true position of the drone at the regular grid position, P, (red crosses of Fig. 2) but give its recorded DGPS position, P', as a random location within a box of dimension (2 x 2 x 5) cm centred at the desired drone location. The simulation then proceeds by determining the 6 'measured' phases by calculating the path difference $D' - R'_n$ and from the wavelength determining a phase. At each 'measurement' point, P', the set of 6 measured phase values are repeated 10 times to account for the phase measurement error. For the simulation each of the 60 phase measurements have a random noise added based on the specified RMS noise level. Repeat for the orthogonal polarisation.

Post processing for a single polarisation *measurement* takes the following form:

- Create the 6 equations of the form of (1) with the unknowns (ϕ_{AUT}, t_x, t_y, t_z) and the chosen values of N_n we apply a Least Squares algorithm using just 4 iterations.
- For each of the 10 cases where a solution is found we test the solution to insure the mean value of the residuals is < 0.1 AND the error vector between the recovered drone location (t_x, t_y, t_z) and the DGPS location is < ε_{lim}. Where ε_{lim} is either the free-space wavelength or the DGPS location maximum error vector (2 x 2 x 5) cm, whichever is the smallest.
- For each valid solution of the 10 cases find the mean values for ϕ_{AUT}, t_x, t_y, t_z. If no valid solutions are found mark this NF point as a *failed* solution.

The simulation then repeats this process for each of the 49 individual drone measurement locations P'.

A. AUT Phase and Drone Position Reconstruction

The AUT phase and drone location recovery process is first tested by taking the known AUT phase such that it produces a linear phase taper in both the x and y dimensions of the measurement plane. The results for the configuration of Fig. 2 are shown in Fig. 3, where 3(a) shows the known true phase at each of the 49 sample points where a high phase taper crossing the ±180° boundary is used to verify that this transition boundary is correctly recovered.

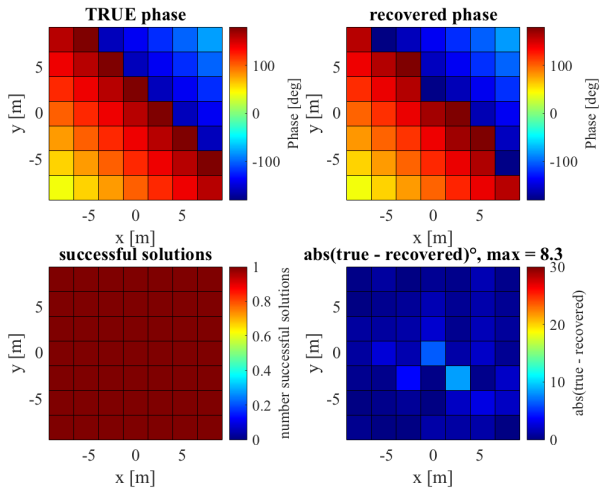

Fig. 3. Results of drone phase recovery for the system of Fig. 2 at 1GHz with a 2° RMS VNA phase measurement error: (a) top left: true phase at measurement points; (b) top right: recovered phase at measurement points; (c) bottom left: successful solutions; (d) bottom right: phase error = abs(true – recovered) with maximum error of 8.3°.

Fig. 3(b) shows the recovered phase, Fig. 3(c) that there is a successful solution at each sample point and Fig. 3(d) the recovered phase error at each sample point, with a maximum error of 8.3° and an RMS error of 1.9°. The recovered drone location error vector had a maximum value of 2.3cm (0.078λ) and an RMS value of 0.7cm (0.023λ), this compares well with the DGPS drone location error vector with maximum of 2.7cm (0.09λ) and RMS value of 1.6cm (0.053λ). There is thus an advantage of using the recovered drone location points for the NF/FF transformation as the position is more accurate. We shall note later that this level of reconstruction accuracy is fairly constant in wavelength terms and so for higher frequencies the improvement in accuracy of recovered drone location provided a very significant and worthwhile improvement. For the cross-polarised component the recovery process is the same. The only limitation on signal amplitude at the measurement point being the signal level at which the VNA measured phases can be accurately made to the desired 2° RMS level.

We next study the effect of the reference antenna location on the AUT phase and drone location recovery process. Just as

in the case of satellite DGPS locations where the best user location accuracy is achieved with a well spread satellite constellation about the user, here a well distributed REF antenna location about the AUT and measurement plane offers the best reconstruction performance.

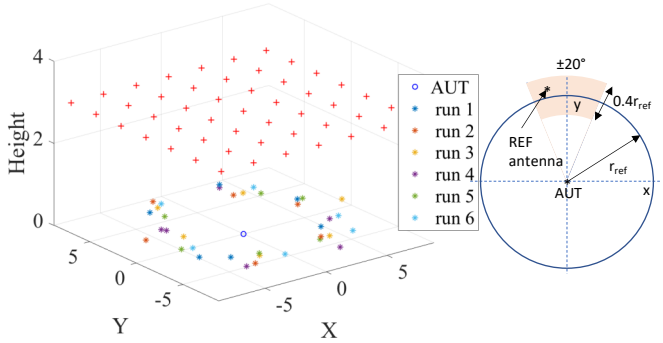

Fig. 4. Left: Six different runs for the 6 REF antenna locations placed around a nominal radius (r_{ref}) of 6.5m. Right: Plan view diagram showing shaded area within which a REF antenna (*) is randomly placed for each run.

To this end, Fig. 4 (left) shows six different runs for the 6 REF antenna locations (labelled *) placed pseudo-randomly around a nominal radius (r_{ref}) of 6.5m. To the right of Fig.4 is a plan view diagram showing the shaded area within which a REF antenna (*) is randomly placed for each run. In addition the height of each REF antenna relative to the AUT is randomly varied over a range 0 to 0.5m. The results for each of these six sets of REF antenna location runs is shown in Fig. 5(a), where each REF antenna set is run 20 times.

Note, each run is subject to the statistics of an RMS phase measurement error of 2° and a DGPS based drone location error of (2 x 2 x 5)cm and the Cumulative Distribution Function (CDF) results for the RMS of the recovered phase over the 49 sample points is shown. Runs 1 and 5 offer the lowest recovered phase error, with runs 2 and 3 worst by a factor of about 2. Fig. 5(b) shows the CDF of recovered RMS phase error with the results of each run shown in Fig. 5(a) plotted at both the 68% CDF and 80% CDF points. Fig. 6(a) shows the corresponding CDF of recovered RMS drone location error vector magnitude (at CDF of 68% and 80%) over the 6 runs of REF antenna locations. Also shown is the CDF of the drone RMS DGPS error location vector, again emphasising the improvement in the reconstructed drone location compared to that from DGPS. Fig. 6(b) shows the reconstruction failure rate (%) for each of the 6 sets of REF antenna locations, indicating that the REF antenna locations of run 5 offer the best performance. Taken over all 6 REF antenna location runs the reconstruction performance was: RMS phase error = 2.3°, drone location error = 0.7cm (0.023λ), failure rate = 0.68%. The results of figures 5 and 6 have shown that there are differences between the performance of the recovery process for the different sets of REF antenna locations with set 5 offering the lowest phase error and failure rate. The importance of using a simulation of the measurement process prior to "live" measurements is clearly demonstrated

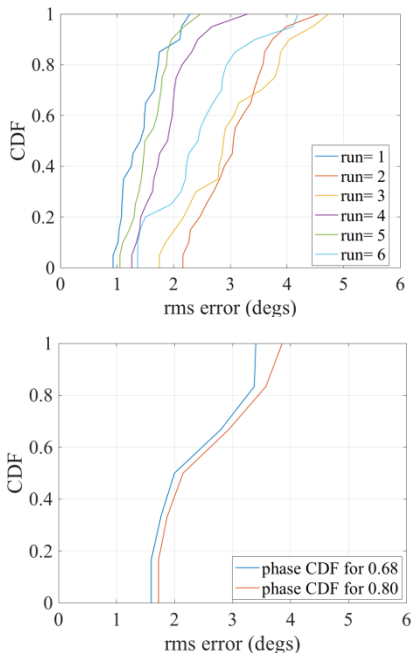

Fig. 5. Results for the six sets of 6 REF antenna location shown in Fig. 4. Frequency 1GHz, RMS phase measurement error of 2°. (a) CDF of recovered RMS phase error over each of the 49 NF sample points. (b) CDF of recovered RMS phase error with the results of each run shown in (a) plotted at both the 68% CDF and 80% CDF points.

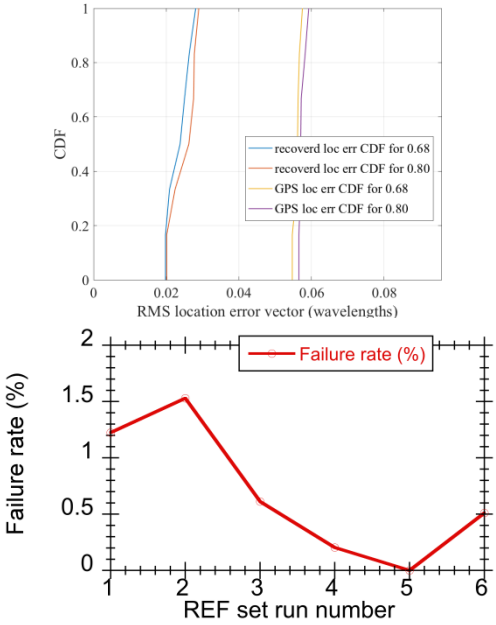

Fig. 6. (a) As Fig. 5b showing CDF of recovered RMS drone location error vector magnitude over the 6 runs of REF antenna locations. Also shown is the CDF of the drone RMS DGPS error location vector. (b) Solution failure rate (%) for each of the 6 sets of REF antenna locations.

We next consider the optimal number of REF antennas and nominal REF antenna location radius (r_{ref}) needed for the reconstruction process.

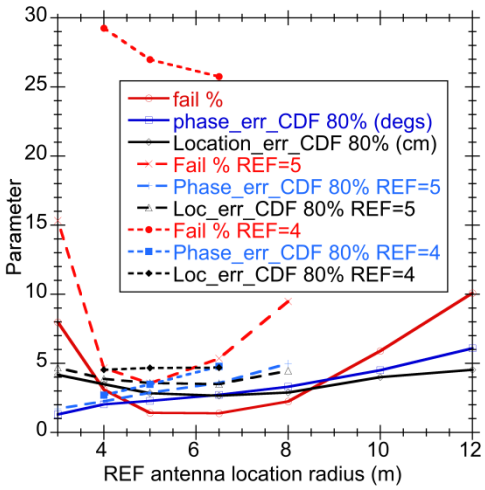

Fig. 7. Comparison of performance for different numbers of REF antenna and different REF antenna location radii (r_{ref}). solid line: REF=6; dash line REF=5; dotted line REF=4. Fail % = Average failure rate of the 6 different REF location runs (red); Phase_err_CDF 80% = RMS phase error at the 80% CDF point (blue); Loc_err_CDF 80% = RMS drone location error vector taken at the 80% CDF point (black).

Fig. 7 compares the % failure rate, the phase error (degrees at CDF of 80%) and the location error vector magnitude (cm at CDF of 80%) for different numbers of REF antennas and values of r_{ref}. Clearly six REF antennas significantly offer the minimal and broadest r_{ref} bandwidth for failure rate (red curves), along with marginally better phase error and error vector magnitude.

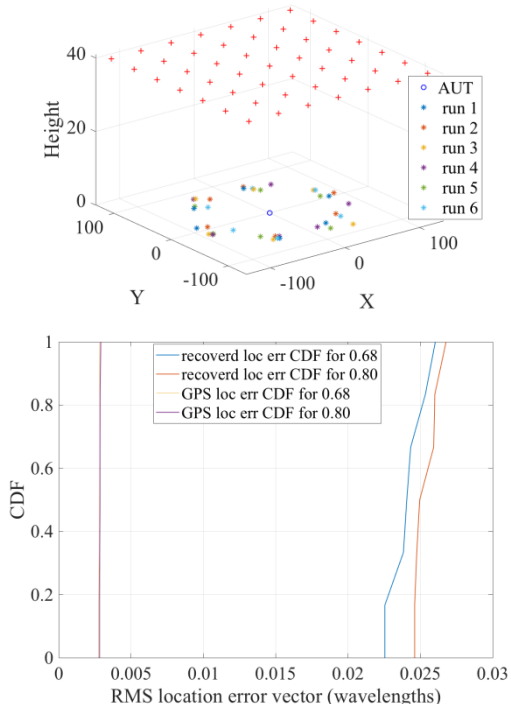

Fig. 8. (a) Measurement system for 50MHz showing six different runs for the 6 REF antenna locations placed around a nominal radius of 80m, RMS phase measurement error used = 2°. (b) CDF of recovered RMS drone location error vector over the 6 sets of REF antenna locations. Also shown is the CDF of the drone RMS GPS error location vector. Failure rate = 2.2%; RMS error of recovered phase over all runs = 1.8°.

The above results have all been undertaken at 1GHz, we now consider the performance at both low and high microwave frequencies. Fig. 8(a) shows the measurement system for operation at 50MHz, again using six different runs for the 6 REF antenna locations placed around a nominal radius (r_{ref}) of 80m and NF scan height of 40m, these increased dimensions reflecting the large (6m) wavelength. The recovered RMS phase error over all six runs remains good at 1.8° (maximum error = 20°), with a failure rate ranging from 0% to 5.4% over the 6 sets of REF antenna locations. Fig. 8(b) shows the CDF of recovered RMS drone location error vector over the 6 sets of REF antenna locations along with the CDF of the drone RMS DGPS location error vector. As the latter is fixed around the 1.6cm level from the DGPS system it is now very small in terms of wavelengths compared to the recovered case which remains at the 0.025λ level. Thus, at this frequency it is clearly better to use the DGPS derived location for the drone, rather than the recovered one. There will clearly be a frequency below which the switch from using the recovered drone position to using the DGPS derived position and this has been found to occur at *circa* 0.5 GHz (GPS location error vector = 0.027λ).

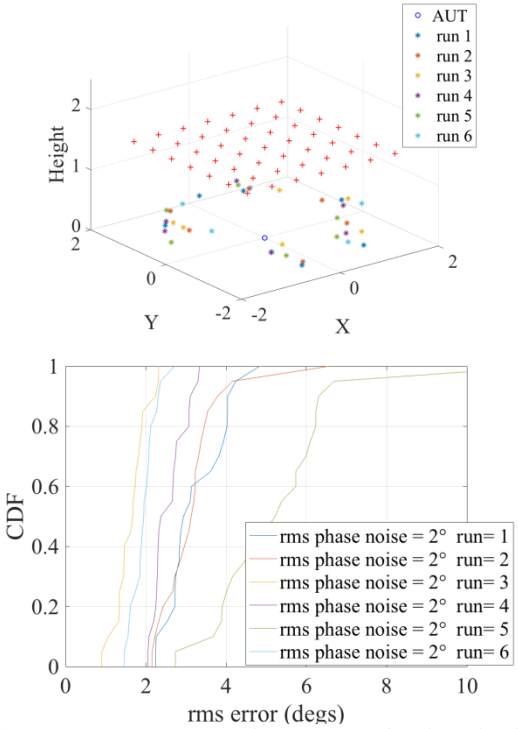

Fig. 9. (a) Measurement system for 12 GHz showing six different runs for the 6 REF antenna locations placed around a nominal radius of 1.5m, RMS phase measurement error used = 2°. (b) CDF of recovered RMS phase error over each of the 49 NF sample points. Failure rate = 5.2%, RMS error of recovered phase over all runs = 3.0°.

Moving to 12 GHz operation, Fig. 9(a) shows the measurement system with NF scan height of 1.5m and r_{ref} = 1.5m, with Fig. 9(b) showing the CDF of recovered RMS phase error over each of the 49 NF sample points for the six sets of REF antenna locations. There is clearly a much wider spread in phase error between the different sets of REF antenna locations, with an average RMS phase error over all sets of 3.0° and an average failure rate of 5.2% (lowest =

4.4%, highest = 5.6%). Again, the recovered RMS drone location error vector remains at around 0.038λ level, but now the RMS DGPS location error vector is at a 0.66λ level, due to the 2.5cm wavelength.

In this section we have demonstrated that using six REF antennas, accurate AUT phase recovery of better than 3° RMS can be achieved over a wide (0.05 to 12) GHz band and that the RMS drone location error can be kept to around the 0.025λ level. In the next section we look at simulations of the full NF to FF measurement system and determine the level of radiation pattern accuracy that can be achieved with the proposed system.

B. Near-Field to Far-Field Antenna Measurement Performance

In this section we model the complete NF/FF drone measurement process, and Fig. 10(a) shows the system used for 1GHz operation using the single beam-formed RF output from a linearly polarised (in x) 28 × 20 element array antenna (elemental dipoles with 0.5λ element spacing) as the AUT. Unlike classical planar NF measurement the drone can easily describe a dome shaped NF measurement surface and this has an advantage in improving the valid FF angle for a given scan radius [13].

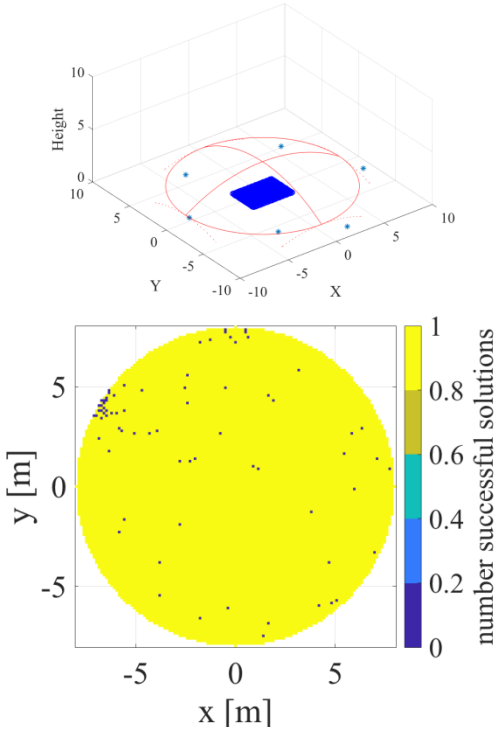

Fig. 10. (a) NF measurement of 28 x 20 array antenna at 1GHz with probe measurements over a spherical cap of radius 15m (shown in red), zenith drone height = 3m, scan radius = 8m, sample spacing over cap = 0.425λ. (b) Sample locations where phase recovery failed giving error rate of 0.58%.

In this case we have taken a spherical cap of radius 15m, and a drone zenith height of 3m, along with an 8m scan radius. To make allowances for the failure rate we have taken a NF sample spacing of 0.425λ. Fig. 10(b) shows a plan view of the scan plane with the sample locations where phase recovery failed shown as blue dots. At these failed sample points we use a complex field interpolation scheme based around the four surrounding sample points to obtain an estimate of the complex field at the location of the failed sample point. The reconstruction failure rate, using an RMS phase measurement error of 2°, over the 16,129 measurements was 0.58%; the RMS phase error was 2.2° (with a maximum error of 18.5°); and the RMS drone location error vector was 0.022λ (with a maximum error of 0.24λ). Fig. 11 compares the FF co-polar pattern of the AUT obtained using the exact NF values (using for example a Plane Wave Spectrum NF/FF transform for non-uniform sample points [5]) with no measurement error (left) to that obtained with the AUT phase recovery and drone position recovery process described in this paper (right hand figure).

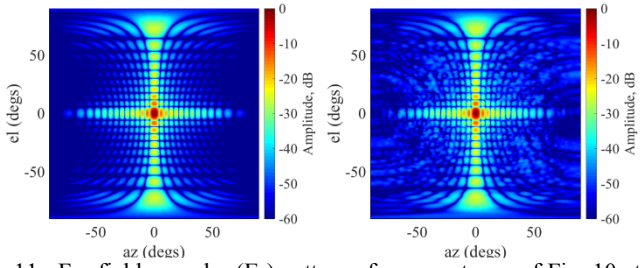

Fig. 11. Far-field co-polar (E_x) pattern of array antenna of Fig. 10 at 1GHz. (left) True pattern. (right) simulated pattern 'measured' by drone with a VNA phase measurement error of 2° RMS.

We have taken the desired location for the sample points to be on a regular grid (the recovered drone locations used in the NF/FF transform are of course on a non-uniform grid), but in practice the desired sample points can form a non-uniform grid to take account of drone dynamics and hence improve flight battery power efficiency. To quantify the level of FF pattern error, Fig. 12a shows the Equivalent Multipath Level (EMPL) [13] for an azimuth radiation pattern cut and Fig. 12b shows the full hemispherical FF pattern EMPL with RMS EMPL level of -57.3dB and this is compatible with what has been reported in an outdoor drone based FF range [4].

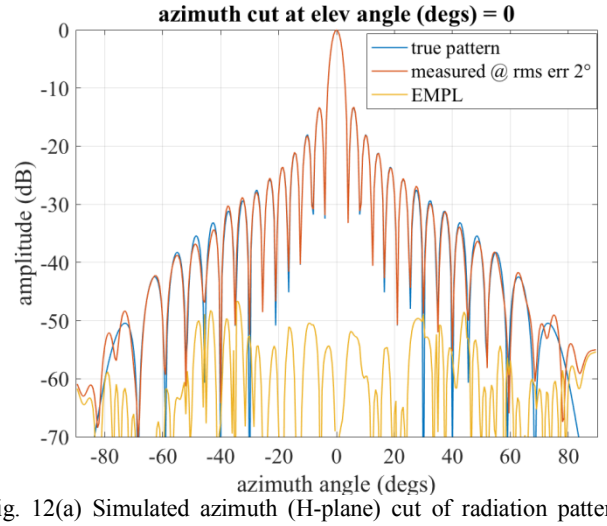

Fig. 12(a) Simulated azimuth (H-plane) cut of radiation pattern of Fig. 11 comparing true and 'measured' plots plus the Equivalent Multipath Level (EMPL).

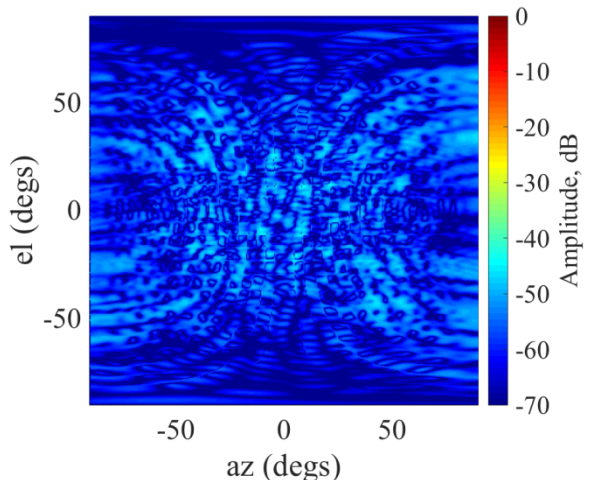

Fig 12(b) Simulated 'Measured' EMPL for whole far-field co-polar (E_x) pattern, RMS EMPL = -57.3dB. VNA phase measurement error of 2° RMS.

We could imagine Fig. 10(a) forming a fixed antenna test facility (fixed: REF antenna locations, AUT location, scan dimensions) and in Table 1 we investigate the facilities bandwidth by measuring the 28 x 20 element array antenna with 0.5λ element spacing at both 0.5GHz and 2GHz. The 0.5GHz results show good performance with an RMS EMPL of -51.3dB and reconstruction failure rate of 0.48% over the 4,225 sample points.

Frequency (GHz)	RMS EMPL (dB)	Failure rate (%)	No. Elements in Array	Drone Zenith (m)	Scan Radius (m)
2.0	-58.2	0.24	28 x 30	3.0	8.0
1.0	-57.3	0.58	28 x 30	3.0	8.0
0.5	-51.3	0.48	28 x 30	3.0	8.0
0.25	-50.7	0.7	14 x 10	3.0	8.0
0.125	-48.2	0.4	7 x 5	6.0	12.0

Table 1. Whole far field co-polar radiation pattern EMPL and failure rate for system shown in Fig. 10. VNA phase measurement error = 2° RMS.

The 2GHz results again show good performance with an RMS EMPL of -58.2dB and reconstruction failure rate of 0.24% over the 64,009 sample points. For higher frequencies, the sample surface needs to be reduced in height and radius to avoid excessive sampling. For lower frequencies the same measurements setup can be used, however a smaller AUT is needed to avoid mechanical interference with the REF antennas. Table 1 also shows results for the system of Fig.10(a) at a frequency of 250MHz using a 14x10 array antenna give an RMS EMPL level of -50.7dB and failure rate of 0.7%. This sets the limit for this system as the drone is now around 3λ from the AUT. Leaving the REF antenna locations unchanged but increasing the drone zenith height to 6m and scan radius to 12m yields the result shown in table 1 for an array antenna of dimension 7x5 at 125MHz. Thus a fixed test facility of the form and size shown in Fig. 10(a) is highly versatile. However, for many applications of this work, where the AUT is to be measured at its installed location the REF antenna locations (in x, y, z) would be determined a-priori from suitable available locations surrounding the in situ AUT and optimised through the use of the measurement systems simulation.

To verify that the system can successfully operate with an array AUT with a phase scanned beam, Fig. 13 compares the 1GHz FF co-polar pattern of array antenna (with beam scanned to 20° azimuth and 10° elevation) obtained using the exact NF values with no measurement error (left) to that obtained with the AUT phase recovery and drone position recovery process (right hand figure). Again, good performance is found with an RMS EMPL of -56.1dB and a failure rate of 0.64%.

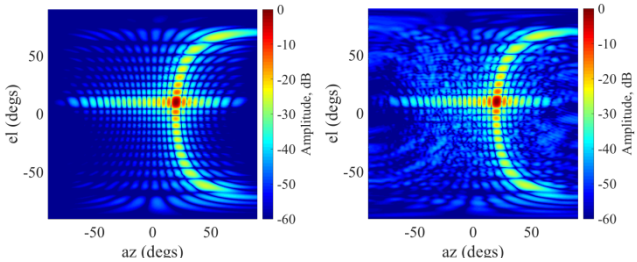

Fig. 13. Far-field co-polar (E_x) pattern at 1GHz as in Fig. 11 but with the array beam scanned to 20° in azimuth and 10° in elevation. True pattern (left), simulated 'measured' pattern (right) EMPL = -56.1dB, failure rate = 0.64%. VNA phase measurement error of 2° RMS.

As described in the introduction to this paper, one motivation for this work was the desire to create an installed performance radiation pattern measurement system for low frequency antennas, such as array antennas used for radio astronomy. Table 2 shows the whole far-field co-polar pattern EMPL and failure rate for a 28 x 20 element array 'measured' at 50 MHz over a spherical cap of radius 160m, with zenith drone height of 30m, scan radius of 80m, r_{ref} of 70m, which is consistent with a potential radio astronomy antenna [2].

Frequency (MHz)	RMS EMPL (dB)	Failure rate (%)	No. Elements in Array	drone zenith (m)	scan radius (m)
50	-56.2	2.1	28 x 30	30.0	80.0
50	-44.9	2.4	7 x 5	30.0	80.0

Table 2. Whole far field co-polar radiation pattern EMPL and failure rate for 50MHz system with NF surface being a spherical cap of radius 160m, zenith drone height = 30m, scan radius = 80m, nominal REF antenna radius = 70m, sample spacing over cap = 0.425λ. VNA phase measurement error = 2° RMS

Table 2 also shows results for the same measurement system to 'measure' the FF of a lower gain 50 MHz array (7x5 elements with 0.5λ element spacing). The authors are not aware of any alternative system that can measure the untethered near-field amplitude and phase of this type of antenna at such low microwave frequencies to this level of EMPL.

We now consider the high frequency performance of the measurement system, with Fig. 14 showing the simulated FF azimuth cut and EMPL levels for a 28x20 array antenna 'measured' at 10 GHz. The system used a flat circular NF sample surface of 1.5m radius with a drone height of 1.5m and r_{ref} of 1.5m. The RMS EMPL for whole FF pattern was -58.1 dB and the reconstruction failure rate was 0.16%.

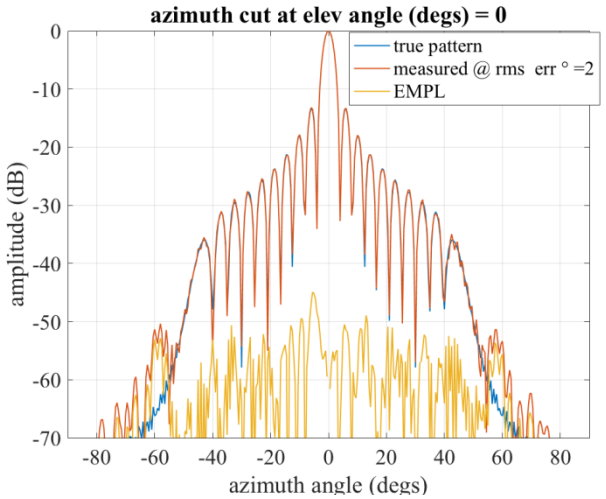

Fig. 14. Simulated azimuth cut of radiation pattern of 28 x 20 element array 'measured' at 10 GHz over a flat NF surface of radius 1.5m, zenith drone height = 1.5m, nominal REF antenna radius = 1.5m, sample spacing over cap = 0.425λ, VNA phase measurement error of 2° RMS.

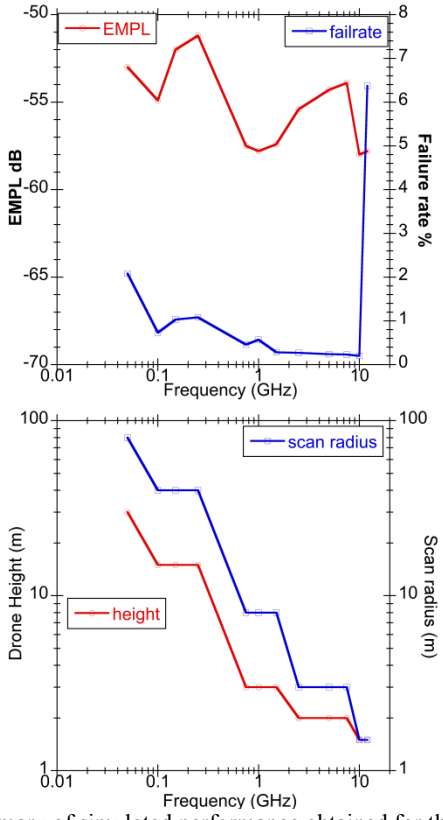

Fig. 15. Summary of simulated performance obtained for the 28x20 array 'measured' from 50 MHz to 12 GHz showing: (a) FF radiation pattern EMPL and reconstruction failure rate, (b) drone zenith height (m) and scan radius (m).

In Fig. 15(a) we summarise the performance in terms of EMPL and reconstruction failure rate of the proposed system over a frequency range of 50MHz to 12GHz. At 12GHz and above we find a rapidly increasing failure rate due to the fact that the error in DGPS location used to give an approximate drone position for the reconstruction process is now very large in wavelength terms (0.64λ at 12GHz). Fig. 15 (b) shows the drone zenith height and scan radius used to obtain the results of Fig. 15(a). Although at 12GHz the failure rate is 6.4%, an EMPL level of -57.8dB was still achieved. Up to this point, all the presented results have been based on the VNA phase measurement error between the AUT and each REF antenna (Fig. 1) being set at 2° RMS. In Fig. 16(a) we explore the dependence on the NF/FF transformed radiation pattern EMPL on the value of the phase measurement error. With the phase error set to zero, the reconstruction is near exact with EMPL levels of -290dB and, as expected, the EMPL increases as phase error increases and the reconstruction failure rate increases rapidly above 3° RMS of phase error.

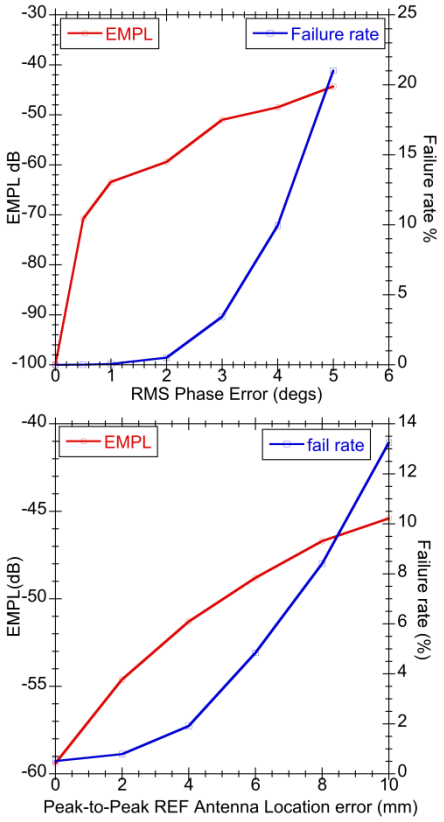

Fig. 16. Effect on FF EMPL level and failure rate of the 28x20 array 'measured' at 1GHz (Fig. 10a) for: (a) different values of RMS VNA phase measurement error; (b) accuracy of determining the location of the six REF antennas.

Also detrimental to the system performance is the accuracy to which the (x, y, z) location of the REF antennas relative to the AUT is known. As described in section 2, this can be measured using a TST with a typical accuracy of about 1.5 mm ± 2 parts per million. With this level of accuracy in mind, Fig. 16(b) shows the effect on FF EMPL level and reconstruction failure rate on the accuracy of determining the location of the 6 REF antennas. An error of 3 mm (0.01λ) has little effect on the EMPL and is in line with what is achievable with a TST. However, this is wavelength dependent, so REF antenna position accuracy will be another limit (together with the DGPS accuracy) to the upper frequency of operation. The alternative use of a laser tracker [31] offers an order of magnitude improvement in accuracy so minimising this limitation. It should be noted that in the analysis of Section 2, the (x, y, z) location of the AUT or REF antennas implies a location based on the antennas phase centre.

This work has concentrated on the recovery of the NF phase and the resulting NF/FF accuracy, the measurement of the NF amplitude would follow the process used in current FF drone measurements, as for example in [4] where the amplitude measurement accuracy of 0.38dB (1σ) was reported, being largely made up of environmental reflections (0.36dB).

Finally, we briefly address the practicality of the proposed measurement system.

Drone based system: The work of [4] has demonstrated the viability of a transmitting drone with gimbal mounted steerable probe antenna and system control electronics. Compact 10MHz to 15GHz dual synthesised source modules of dimension (90 x 50 x 19)mm are commercially available [20] and suitable probe antennas include: dual Vivaldi [21], tapered slot [25], or broadband biconical [22].

Ground based system: REF antennas should offer a broad radiation pattern with stable phase performance and so circularly polarised (CP) antennas of the type used for GPS ground terminals are suitable to receive the linearly polarised drone-based probe signal, see for example [23]. As stated in [25] the desired drone-based probe shall be dual-polarised, broadband, light in weight, mechanically stable, compact in size, least affected by wind and electromagnetically insensitive to the UAV, and this reference proposes a very suitable tapered slot probe antenna design. As stated in section II we propose that the drone-based probe antenna will always point towards the AUT using a tracking system [4], so probe compensation is limited to polarisation alignment in the NF/FF process. The phase radiated by the probe at each REF antenna needs to be adjusted for radiated phase pattern of the probe antenna, and this is simply achieved within the reconstruction software as the geometry of the complete probe REF antenna system is fully known. In the above simulations we have chosen to locate the 6 REF antennas randomly in height to within a couple of wavelengths. This is not a necessary requirement as the REF antennas can be located around the AUT at any height so long as their coordinates are accurately determined, hence enabling in-situ AUT measurements. A preliminary power budget for the drone (0.1W transmit power and antenna gain of 3dBi) to a single REF antenna (gain of 3dBi) including cabling loss to the VNA located near to the AUT (see Fig. 1) indicates a SNR for 100 Hz intermediate frequency bandwidth (IFBW) of 39.2dB, 47.6dB, 41.7dB for the systems studied at (0.05, 1.0, 10.0) GHz respectively. A similar calculation for the drone to AUT (gain of 20dBi) at a signal level -40dB down from the peak NF level indicates a SNR for 100 Hz IFBW of 37.7dB, 31.7dB, 23.2dB for the systems studied at (0.05, 1.0, 10.0) GHz respectively. Based on the noise levels of both these paths the VNA measured RMS phase noise between AUT and REF antenna would then be (1.7°, 1.7°, 2.2°) at (0.05, 1.0, 10.0) GHz respectively, justifying our conservative choice of 2° RMS as the baseline error level across the whole dynamic range of the NF.

Whilst this work has concentrated on the application of the technique to drones, the increasing use of multi-axis, industrial robots as a means of providing NF probe scanning offers an additional application. A major limitation in the use of industrial robots for NF probe positioning is that the construction of the multiple rotational joints of the arm prohibits access to rotary RF joints and so RF phase stable cable management from robot base to robot head becomes a significant issue at 30 GHz and above. Taking a 40 GHz measurement as an example, and assuming a (pessimistic) robotic arm positional accuracy of 2mm in (x, y, z), plus a REF antenna position accuracy of 0.2mm (0.025λ), Fig. 17 shows an azimuthal cut for 40GHz with an whole pattern RMS EMPL of -46.6dB and 0.2% failure rate. With REF antenna position accuracy increased to 0.1mm RMS EMPL improves significantly to -52.6dB and failure rate remains at 0.2%. We note that positional accuracy of 0.1mm is easily achievable over this compact test setup using a 3D laser tracker [13].

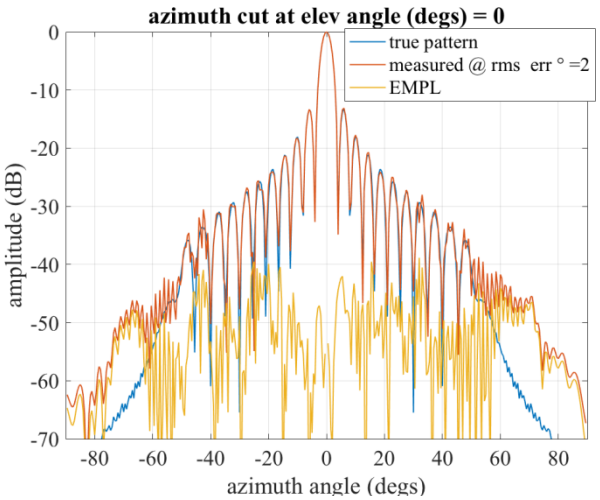

Fig. 17. Simulated azimuth cut of radiation pattern of the 28 x 20 element array 'measured' at 40 GHz over a scan radius 0.5m, robotic arm zenith height 0.4m, nominal REF antenna radius = 0.5m, REF antenna position accuracy 0.2mm (0.025λ), VNA phase measurement error of 2° RMS.

IV CONCLUSIONS

Through simulation this work has demonstrated that the use of six reference antennas and a multichannel VNA can enable untethered drone-based NF/FF antenna measurements to be achieved with a high level of accuracy. The technique, based on the principles of GPS, recovers the phase of the AUT at each NF probe point as well as the true location of the probe (drone). This process of phase recovery via reference antennas has the added bonus that long term phase drift, often a NF acquisition problem, is removed. The work is particularly applicable to VHF/UHF antennas and we have demonstrated that a 28 x 20 element land-based array can be measured at 50 MHz at a drone altitude of 30m. An example measurement 'range' (comprising AUT location and six fixed REF antennas) has been shown to offer a wide operating bandwidth for the AUT of (0.5 to 2) GHz, with EMPL < -50dB. In the case of large antenna farms it is often not possible to tilt an antennas elevation down sufficiently low for unobstructed slant range FF drone based measurements. The authors are not aware of any alternative system that can measure the untethered near-field amplitude and phase of these types of antenna to this level of accuracy.

We have investigated the various errors involved, including VNA phase measurement accuracy (2° RMS), REF antenna

location accuracy (0.01λ). It has been shown that the DGPS accuracy that is used to give an estimate to the true location of the drone limits the upper frequency of operation to about 10GHz. However, above this frequency, direct far-field drone measurements have been demonstrated to be viable [4]. In addition, we have shown the technique is applicable to small indoor NF measurements using an industrial robotic arm for probe placement, where the accuracy of the probe location is much higher (2mm peak-to-peak), and in such cases a 40GHz NF/FF measurement is possible with EMPL < -50dB.

The primary advantage of the proposed system is to obtain an accurate determination of the AUT NF phase without the use of optical fibre cable tethers or additional NF scans. As a bi-product of the multiple reference antenna approach an improved determination of the location of the drone-based probe antenna over that offered by DGPS is achieved. The accuracy of the reconstructed phase and drone-based probe location is dependent on two key factors: the accuracy to which the VNA can measure the REF_n to AUT phase in the presence of noise and the accuracy to which the approximate location, *P'*, of the drone-based probe can be determined which is used to drive the solution search. We have shown that using DGPS to determine *P'*, limits the upper frequency of operation to circa 10GHz. If we can determine *P'* more accurately there is a corresponding increase in the upper frequency of operation, and this has been demonstrated where a robotic arm is used to give an order of magnitude improvement in location accuracy of *P'* and operation at 40 GHz. If the above referenced use of laser trackers to determine drone location *P'*, rather than DGPS, becomes viable with submillimetre accuracy then a further order of magnitude increase in the upper frequency bound results and the system becomes viable for all microwave and millimetrewave antennas.

In summary the proposed system is compatible with current DGPS based drone location technology and can exploit the improved accuracy offered by laser trackers whilst offering cable-free untethered movement of the probe antenna. We have shown that the location of the REF antennas is flexible and is hence compatible with in-situ antenna testing, which is seen as one of the major advantages of drone-based NF/FF testing.

The next phase of this work will be implementation of the system with both drone and robotic arm based acquisitions, as well as investigating a calibration process to remove the need for high accuracy in the location of the REF antennas.

V. REFERENCES

[1] María García-Fernández; et al, "Antenna Diagnostics and Characterization Using Unmanned Aerial Vehicles", IEEE Access, Year: 2017 | Volume: 5.

[2] Fabio Paonessa; et al, "UAV-based pattern measurement of the SKALA", 2015 IEEE International Symposium on Antennas and Propagation & USNC/URSI National Radio Science Meeting

[3] Torsten Fritzel; Hans-Jürgen Steiner; Rüdiger Strauß, " Advances in the Development of an Industrial UAV for Large-Scale Near-Field Antenna Measurements", 2019 13th European Conference on Antennas and Propagation (EuCAP).

[4] Cosme Culotta-Lopez; et al, "On the Uncertainty Sources of Drone-Based Outdoor Far-Field Antenna Measurements", 2021 Antenna Measurement Techniques Association Symposium (AMTA), Daytona Beach, FL, USA, Oct. 2021.

[5] C. G. Parini, S. F. Gregson, J. McCormick, D. Janse van Rensburg, Thomas Eibert, "Theory and Practice of Modern Antenna Range Measurements, Second edition ", Vols. 1 and 2, IET Press, 2021, ISBN 978-1-83953-126-2.

[6] Raimund A. M. Mauermayer; et al, "A Low-Cost Multicopter Based Near-Field Antenna Measurement System Employing Software Defined Radio and 6-D Laser Metrology", 2019 Antenna Measurement Techniques Association Symposium (AMTA).

[7] Hans-Jürgen Steiner;Torsten Fritzel;Rüdiger Strauß, "Aspects of Near-Field Antenna Measurement Technology when using UAV's", 15th European Conference on Antennas and Propagation (EuCAP), 2021.

[8] A. Weiß; et al, "RF-Signal Receiver for UAV-Based Characterisation of Aeronautical Navigation Systems", 14th European Conference on Antennas and Propagation (EuCAP), 2020.

[9] María García-Fernández; et al, "Evaluation of an Unmanned Aerial System for Antenna Diagnostics and Characterization", 2018 12th European Conference on Antennas and Propagation (EuCAP).

[10] L. Ciorba; et al, "Near-Field Phase Reconstruction for UAV-based Antenna Measurements", 2019 13th European Conference on Antennas and Propagation (EuCAP).

[11] Quentin Gueuning; et al, "Plane-wave spectrum methods for the near-field characterization of very large structures using UAVs: The SKA radio telescope case", 15th European Conference on Antennas and Propagation (EuCAP), 2021.

[12] Fabian T. Faul, Thomas F. Eibert, "Setup and Error Analysis of a Fully Coherent UAV-based Near-Field Measurement System", 15th European Conference on Antennas and Propagation (EuCAP), 2021.

[13] Torsten Fritzel; Hans-Jürgen Steiner; Rüdiger Strauß, "Laser tracker metrology for UAV-based antenna measurements", IEEE Conference on Antenna Measurements & Applications (CAMA), 3-6 Sept. 2018, DOI: 10.1109/CAMA.2018.8530613

[14] Patrick Henkel; et al, "Precise 6D RTK Positioning System for UAV-based Near-Field Antenna Measurements",14th European Conference on Antennas and Propagation (EuCAP), 2020.

[15] W.H. Press; et al, "Numerical Recipes in Fortran", Second Edition, Cambridge University Press, 1992, ISBN 0-521-43064-X.

[16] "ZNBT Vector Network Analyzer: Specifications", Rohde & Schwarz, April 2020.

[17] Streamline Series Vector Network Analyzer (A-models) 2/4-port Up to 53 GHz. 2/4/6-port Up to 20 GHz, Keysight Technologies, data sheet 2021.

[18] Jacquelyne Ta, "Global Positioning System", A Thesis Presented to The Faculty of the Mathematics Program California State University Channel Islands, Degree Masters of Science, April, 2011.

[19] Kavanagh, B. F.; Bird, S. J. G., "Surveying: Principles and Applications", (4th ed.), Prentice Hall, 1996, pp. 257–264, ISBN 9780134383002.

[20] SynthHD (v2): 10MHz – 15GHz Dual Channel Microwave Generator, Windfreak Technologies, LLC, https://windfreaktech.com/product/microwave-signal-generator-synthhd/

[21] Tescom Dual Polarized Vivaldi Antenna, TC-93083A, http://en.tescom.co.kr/product/product4?code=040204

[22] Aaronia BicoLOG 30100 X Biconical Broadband Antenna, https://aaronia-shop.com/products/emc-antenna-bicolog-30100.

[23] Yuan-Ming Cai, Ke Li, Ying-Zeng Yin, and Xueshi Ren, "Dual-Band Circularly Polarized Antenna Combining Slot and Microstrip Modes for GPS With HIS Ground Plane", IEEE Antennas And Wireless Propagation Letters, VOL. 14, 2015.

[24] T. Satoh and A. Ogawa, "Exact gain measurement of large aperture antennas using celestial radio sources," IEEE Transactions on Antennas and Propagation, vol. 30, no. 1, pp. 157-161, January 1982, doi: 10.1109/TAP.1982.1142746.

[25] Arslan Azhar; Thomas F. Eibert, "A Dual-Polarized Tapered Slot Antenna for UAV-Based Collection of Locally Coherent Field Data", 15th European Conference on Antennas and Propagation (EuCAP), 2021.

[26] Fernando Rodríguez Varela;Belén Galocha Iragüen;Manuel Sierra Castañer, "Single-Cut Phaseless Near-Field Measurements for Fast Antenna Testing", IEEE Transactions on Antennas and Propagation, 2022.

[27] M García Fernández, Y Álvarez López, F Las-Heras, "Dual-probe near-field phaseless antenna measurement system on board a UAV", Sensors, Oct. 2019, mdpi.com

[28] Alexander Paulus; Josef Knapp; Jonas Kornprobst; Thomas F. Eibert, "Reliable Linearized Phase Retrieval for Near-Field Antenna Measurements with Truncated Measurement Surfaces", IEEE Transactions on Antennas and Propagation, 2022.
[29] Fabian T. Faul; Thomas F. Eibert, "Setup and Error Analysis of a Fully Coherent UAV-based Near-Field Measurement System", 15th European Conference on Antennas and Propagation (EuCAP), 2021
[30] XL. Ciorba; et al, "Near-Field Phase Reconstruction for UAV-based Antenna Measurements", 13th European Conference on Antennas and Propagation (EuCAP), 2019.
[31] FARO® Vantage Laser Trackers with 6DoF Probe, data sheet, https://knowledge.faro.com, 2022.
[32] D. A. Guidice; J. P. Castelli, "The Use of Extraterrestrial Radio Sources in the Measurement of Antenna Parameters", IEEE Transactions on Aerospace and Electronic Systems, Volume: AES-7, Issue 2, 1971.
[33] S. F. Gregson, J. McCormick, & C. G. Parini, "Principles of Planar Near Field Antenna Measurement", IET Electromagnetics Series, December 2007.